Reduction of Fe(III) colloids by Shewanella putrefaciens: a kinetic model.

Bonneville, S.; Behrends, T.; van Cappellen, P.; Hyacinthe, C.; Roling, W.F.M.

published in
Geochimica et Cosmochimica Acta
2006

DOI (link to publisher)
10.1016/j.gca.2006.04.029

document version
Publisher's PDF, also known as Version of record

Available online at www.sciencedirect.com
ScienceDirect
Geochimica et Cosmochimica Acta 70 (2006) 5842–5854
Geochimica
www.elsevier.com/locate/gca

Reduction of Fe(III) colloids by *Shewanella putrefaciens*: A kinetic model

Steeve Bonneville [a,*], Thilo Behrends [a], Philippe Van Cappellen [a], Christelle Hyacinthe [a], Wilfred F.M. Röling [b]

[a] *Department of Earth Sciences—Geochemistry, Faculty of Geosciences, Utrecht University, P.O. Box 80.021, TA 3508 Utrecht, The Netherlands*
[b] *Department of Molecular Cell Physiology, Faculty of Earth and Life Sciences, Vrije Universiteit Amsterdam, Amsterdam, De Boelelaan 1087, 1081 HV Amsterdam, The Netherlands*

Received 20 November 2005; accepted in revised form 11 April 2006

Abstract

A kinetic model for the microbial reduction of Fe(III) oxyhydroxide colloids in the presence of excess electron donor is presented. The model assumes a two-step mechanism: (1) attachment of Fe(III) colloids to the cell surface and (2) reduction of Fe(III) centers at the surface of attached colloids. The validity of the model is tested using *Shewanella putrefaciens* and nanohematite as model dissimilatory iron reducing bacteria and Fe(III) colloidal particles, respectively. Attachment of nanohematite to the bacteria is formally described by a Langmuir isotherm. Initial iron reduction rates are shown to correlate linearly with the relative coverage of the cell surface by nanohematite particles, hence supporting a direct electron transfer from membrane-bound reductases to mineral particles attached to the cells. Using internally consistent parameter values for the maximum attachment capacity of Fe(III) colloids to the cells, M_{max}, the attachment constant, K_P, and the first-order Fe(III) reduction rate constant, k, the model reproduces the initial reduction rates of a variety of fine-grained Fe(III) oxyhydroxides by *S. putrefaciens*. The model explains the observed dependency of the apparent Fe(III) half-saturation constant, K_m^*, on the solid to cell ratio, and it predicts that initial iron reduction rates exhibit saturation with respect to both the cell density and the abundance of the Fe(III) oxyhydroxide substrate.

1. Introduction

The dissimilatory reduction of ferric iron is an important geomicrobial process in soils, sediments, aquifers, and stratified water bodies, where it relies primarily on Fe(III) oxyhydroxide minerals as terminal electron acceptors (Canfield et al., 1993; Albrechtsen and Christensen, 1994; Taillefert et al., 2000). In addition to being an important oxidation pathway of organic matter and generating soluble ferrous iron, microbial iron reduction can have a major impact on the persistence and mobility of metals, radionuclides, and organic contaminants under anoxic conditions (Lovley et al., 1993; Lovley and Coates, 1997; Anderson and Lovley, 1999; Cummings et al., 1999; Zachara et al., 2001; McCormick et al., 2002; Behrends and Van Cappellen, 2005). A particular challenge facing iron reducing microorganisms is the very low solubility of Fe(III) oxyhydroxides under near-neutral pH conditions. The simplest strategy to overcome this limitation is for the microorganisms to associate directly with the mineral surfaces (Arnold et al., 1988; Caccavo, 1999; Caccavo and Das, 2002). In the absence of direct cell–mineral contact, soluble electron shuttles or chelating agents are needed to transfer electrons from membrane-bound electron transport proteins to Fe(III) (Kappler et al., 2004).

In a recent study, we showed that the initial reduction kinetics of a variety of Fe(III) oxyhydroxides by the iron reducing bacterium *Shewanella putrefaciens* systematically exhibit saturation with respect to the Fe(III) substrate availability (Bonneville et al., 2004). The observed parabolic

* Corresponding author. Fax: +31 30 253 5302.
E-mail address: s.bonneville@geo.uu.nl (S. Bonneville).

0016-7037/$ - see front matter © 2006 Elsevier Inc. All rights reserved.
doi:10.1016/j.gca.2006.04.029

dependence of the Fe(III) reduction rate on the mineral concentration could be fitted to the Michaelis–Menten rate equation, yielding a maximum reduction rate per cell, v_{max}, and an apparent half-saturation constant, K_m^*. The value of v_{max} was found to be characteristic of the oxyhydroxide mineral undergoing reduction, generally increasing with increasing mineral solubility (Bonneville et al., 2004).

Our previous experimental results, and evidence from other studies (Das and Caccavo, 2000; Caccavo and Das, 2002), indicate that the reduction of iron oxyhydroxides by *S. putrefaciens* occurs predominantly via the transfer of electrons to Fe(III) centers at the cell–mineral interface. When the cell surface is saturated by the solid-state Fe(III) substrate, the iron reducing activity of *S. putrefaciens* reaches its maximum value, v_{max}. Further increasing the concentration of the Fe(III) substrate then no longer has an effect on the rate of iron reduction. This saturation behavior is captured by the Michaelis–Menten rate equation.

The usual form of the Michaelis–Menten rate equation for enzymatic reactions assumes that the enzyme concentration is small with respect to the substrate concentration. The amount of substrate associated with the enzyme can then be neglected, and the total and free concentrations of the substrate are almost identical. For a dissolved substrate, this simplification is usually adequate, and the half-saturation constant is uniquely defined when expressed in terms of bulk substrate concentration units. Its value provides a direct measure of the affinity of the enzyme to combine with the substrate.

The reduction of Fe(III) oxyhydroxide minerals by *S. putrefaciens* presents a more complex situation, however. The Fe(III) centers that can undergo reduction are located in the contact region between cell and mineral. The direct Fe(III) substrate therefore only represents a fraction of the bulk Fe(III) in the system. Furthermore, under typical experimental conditions, the approximation that the amount of Fe(III) associated with cells is negligible, compared to the total amount of Fe(III), may not be valid. As a result, K_m^* values expressed in units of bulk concentration of the Fe(III) substrate (e.g., in moles of Fe(III) per unit volume mineral–cell suspension) are conditional, rather than intrinsic, kinetic parameters. For instance, in our earlier study, K_m^* values were shown to depend on the solid-to-cell ratio of the experimental suspensions (Bonneville et al., 2004).

The present study explicitly links the association of mineral particles and iron reducing microorganisms to the rate of dissimilatory iron reduction, using suspensions of *S. putrefaciens* and nanoparticulate hematite as model experimental system. Iron reduction rates measured in the presence of excess electron donor are related to the relative coverage of the cells by the iron colloids. Based on the results, a kinetic model for the microbial reduction of nanohematite is developed, which takes into account the abundance and size of the mineral particles. The predictive capability of the model is tested by extending it to a number of other colloidal Fe(III) oxyhydroxides.

2. Materials and experimental methods

2.1. Fe(III) oxyhydroxides

Hematite nanoparticles were prepared by adding 100 mL of a 0.1 M $Fe(NO_3)_3$ solution at a flow rate of 3 mL min^{-1} to 1 L of boiling and vigorously stirred demineralized water (Liger, 1996). After allowing the hematite suspension to cool down to room temperature, it was dialyzed in demineralized water adjusted to pH 4 with 0.5 M HCl, in order to remove the nitrate. Thereafter, the mineral suspension was filtered successively through 0.45 and 0.2 μm pore size filters (Millipore). The average grain size of the hematite nanoparticles, measured using electron transmission microscopy (TEM), was 8 nm (±2 nm). X-ray diffraction and ^{57}Fe Mossbauer spectroscopy analyses revealed highly crystalline hematite with trace amounts of ferrihydrite (Dr. D. Rancourt, University of Ottawa, personal communication). A surface site density of 2.07 sites per nm^2 and a pH of zero net proton charge of 8.15 were derived from acid–base titrations (Liger et al., 1999).

Amorphous ferric oxide (HFO) and ferrihydrite 6 lines were prepared following the procedures described in Bonneville et al. (2004). Lepidocrocite (Bayferrox 943) and low surface area (LSA) hematite (Bayferrox 105M) were purchased from Harold Scholz & Co., GmbH, and used as received. The grain size and shape (obtained using TEM), and the specific surface area (measured by N_2 BET) of the different Fe(III) oxyhydroxides are listed in Table 1.

Table 1
Properties of the Fe(III) oxyhydroxides

Iron oxyhydroxide	Dimensions (nm)	Shape	Surface area ($m^2\ g^{-1}$)	v_{max}[a] (10^{-11} μmol h^{-1} $cell^{-1}$)
Nanohematite	8	Sphere	125	2.4
6-Line ferrihydrite	8	Sphere	175	8.1
LSA[b] hematite	90	Sphere	12	0.27
Lepidocrocite	50 × 300	Needle	83	2.0
HFO[c]	1.3	Sphere	600	6.5

[a] Maximum cell-normalized iron reduction rate by *S. putrefaciens* in the presence of excess lactate (from Bonneville et al., 2004).
[b] LSA = low surface area.
[c] HFO = hydrous ferric oxide.

2.2. Bacteria

Cultures of *S. putrefaciens* 200R were provided by Dr. T. DiChristina, Georgia Institute of Technology (DiChristina and DeLong, 1994; DiChristina et al., 2002). Cells were kept aerobically on Luria–Bertani (LB) medium plates (Tryptone–water 15 g L^{-1}, agar 15 g L^{-1}, NaCl 5 g L^{-1}, and yeast 5 g L^{-1}) and routinely cultured in liquid LB medium on a rotary shaker (150 rpm) at room temperature. The bacteria were harvested in the late exponential-early stationary growth phase based on preliminary culturing experiments where the bacterial density was monitored over time under exactly the same conditions. The cells were washed with 10 mM NaCl solution, followed by centrifugation (6800*g*) and resuspension. The washing procedure was repeated three times. After the last centrifugation step, cells were concentrated in 50 mL of 10 mM NaCl solution. The bacteria were harvested and washed just before being used in the experiments.

Cell numbers were determined by epifluorescence microscopy after acridine orange staining (Hobbie et al., 1977): 100 μL of bacterial suspension were mixed with 4.4 mL of phosphate buffer solution (8 g L^{-1} NaCl, 2 g L^{-1} KCl, 1.44 g L^{-1} Na_2HPO_4, and 0.24 g L^{-1} KH_2PO_4), 200 μL of a 0.25 g L^{-1} acridine orange solution and 0.5 mL of a 30% formaldehyde solution. After 10 min, 100–200 μL of the suspension was transferred to a 17 mm diameter filter tower to which 5 mL phosphate buffer solution and 200 μL of acridine orange solution were added in advance. The content of the tower was mixed by swirling and then filtrated through a black 0.2 μm polycarbonate filter (Millipore). An epifluorescence microscope equipped with a camera was used to take five pictures of each filter. The counting of the cells was performed automatically using imaging software.

2.3. Microbial attachment and reduction of nanohematite

Attachment of nanohematite particles to *S. putrefaciens* cells was measured under aerobic conditions and in the absence of electron donor. Concentrated cell suspensions of *S. putrefaciens* were added to nanohematite suspensions giving a final volume of 50 mL. The suspensions were prepared in 5 mM NaCl solutions, whose pH was adjusted to 5 using HCl. Preliminary tests showed that under these conditions the nanohematite particles formed stable colloidal suspensions. The absence of aggregation was a prerequisite for separating nanohematite particles attached to bacteria from those remaining as free colloids.

The attachment experiments were performed at three cell densities (3.0×10^8, 1.0×10^9, and 1.25×10^9 cells mL^{-1}), while the nanohematite concentration was varied from 25 to 2820 μmol Fe(III) L^{-1}. After 4 h of continuous agitation on a horizontal shaker, aliquots of the suspensions were centrifuged at 900*g* for 40 min. In preliminary experiments, this centrifugation procedure was shown to quantitatively pelletize the bacterial cells (>97% recovery), while avoiding sedimentation of free nanohematite particles (<9% loss). In a limited number of cases, aliquots of cell–mineral suspensions were periodically sampled over the duration of an experiment, in order to follow the time-dependent attachment of nanohematite colloids to the cells.

Total Fe(III) concentrations in the aliquots were determined before and after centrifugation: 750 μL of suspension was mixed with 250 μL of 2 M HCl and kept at 60 °C overnight in order to completely dissolve the nanohematite. Hydroxylamine hydrochloride solution (1.4 M in 2 M HCl) was then added to reduce Fe(III) to Fe(II), followed by the determination of total iron concentration by ferrozine essay (Viollier et al., 2000). The amount of hematite attached to the bacteria was calculated from the difference between the iron concentrations measured before and after centrifugation.

The attachment experiments were directly followed by microbial Fe(III) reduction experiments. After centrifugation, the suspension of free nanohematite colloids overlying the pellet was decanted. The pellet, containing the bacterial cells with attached nanohematite, was resuspended in a medium of 10 mM lactate, 5.6 mM KCl, 14 mM Na_2SO_4, 20 mM NH_4Cl, 1.2 mM $CaCl_2{\cdot}6H_2O$, 1 mM $MgSO_4$, and 10 mM Hepes buffer. The medium pH was adjusted to 7. The incubation experiments were performed in 100 mL septum bottles under anaerobic conditions at room temperature (22 °C). The bottles were kept on a rotary shaker and sampled regularly during 250 h. Concentrated HCl was added to the samples to a final concentration of 0.5 M HCl. After 1 h, the total Fe(II) concentration was measured, following the method of Viollier et al. (2000). The measured total Fe(II) concentration included in dissolved Fe(II) as well as Fe(II) sorbed to the nanohematite or the bacteria.

2.4. Detachment experiments

The reversibility of nanohematite attachment to cells of *S. putrefaciens* was tested in three sets of seven experiments. Each experimental set was carried out with a different concentration of nanohematite (2044, 1089, and 102 μM Fe(III)), exposed to a bacterial density of 2.8×10^8 cells mL^{-1}. Attachment of nanohematite to the bacteria followed the procedure described in Section 2.3. After centrifugation, pellets containing bacteria and attached nanohematite were resuspended under aerobic conditions in 5 mM NaCl solution at seven different pH values: 5, 5.5, 6, 6.5, 7, 8, and 9. No electron donor was added to the experimental media. The bottles were kept on a shaking table under aerobic conditions; samples were collected 10 min and 24 h after resuspending the bacteria. The samples were filtered through 0.2 μm pore size filters to retain bacterial cells and attached nanohematite particles. Total Fe(III) concentrations in the filtrate solution were measured as described in Section 2.3. The amount of nanohematite detached from

the cells was calculated as the difference between the initial amounts of hematite attached at pH 5 and that remaining after 24 h of resuspension in 5 mM NaCl solution at variable pH.

3. Experimental results

3.1. Nanohematite attachment to S. putrefaciens

The results of the 25 individual attachment experiments are summarized in Fig. 1. At low mineral to cell ratios ($<5\times10^{-10}$ μmol Fe(III) cell^{-1}), on the order of 90% of the added nanohematite was associated with the bacteria. With increasing mineral loading, the cell-normalized amount of attached nanohematite ultimately reached a maximum value. The observed saturation of the cells with nanohematite for three bacterial densities could be fitted to a Langmuir isotherm (Fig. 1), with average values for the attachment constant, K_P, of 2.0×10^{-2} L μmol^{-1} Fe(III) and the maximum attachment capacity on the cells, M_{max}, of 1.1×10^{-9} μmol Fe(III) cell^{-1}. Fitting of the Langmuir isotherm to the data for the individual cell densities yielded ranges for the parameters values of 0.8–1.4 × 10^{-9} μmol cell^{-1} (M_{max}) and 1.0–5.3 × 10^{-2} L μmol^{-1} (K_P).

The attachment kinetics were fast with little change in the cell-bound nanohematite concentration beyond the first 10 min after adding cells to the colloidal hematite suspensions (results not shown). Furthermore, in all of the 21 detachment experiments, less than 10% of nanohematite was recovered in the filtrates after 24 h, irrespective of the medium pH (pH range 5–9, results not shown). Especially under acid conditions (pH 5–6), no evidence for coagulation of nanohematite was found. Therefore, retention of nanohematite on the filters most likely reflected cell-bound mineral particles. Thus, the nanohematite particles appeared to be strongly bound to the surface of *S. putrefaciens*. Henceforth, it was assumed that nanohematite colloids attached to the cells at pH 5 remained cell bound during the subsequent reduction experiments at pH 7.

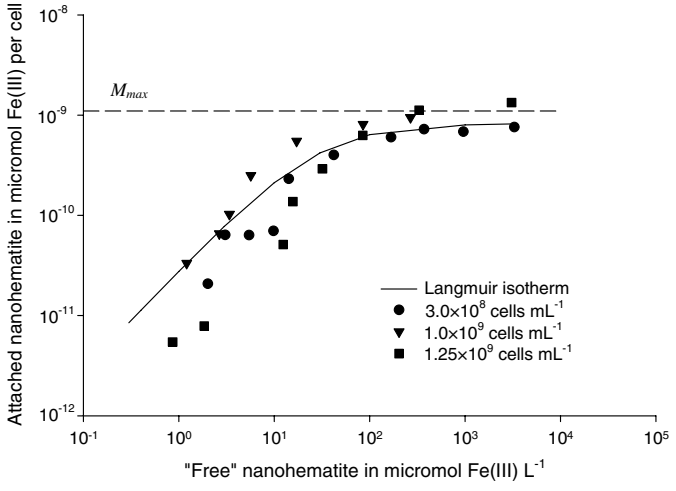

Fig. 1. Attachment of nanohematite to *S. putrefaciens* 200R, upon exposure of three bacterial densities (3.0×10^8, 1.0×10^9, 1.25×10^9 cells mL^{-1}) to a range of total nanohematite concentrations (from 25 to 2820 μmol Fe(III) L^{-1}) in 5 mM NaCl, at pH 5. The horizontal axis corresponds to the concentration of nanohematite particles that do not attach to the cells. The solid line is the best-fit Langmuir isotherm to the entire data set. The dashed line is the M_{max} value derived from this fit.

3.2. Nanohematite reduction by S. putrefaciens

Upon resuspension of cells with attached nanohematite in lactate-containing, pH 7, medium, Fe(II) started building up after a lag time on the order of 24 h (Fig. 2a). The Fe(II) concentration then increased near-linearly for about 200 h (Fig. 2a), followed by a progressive slowing down of the rate of Fe(II) production (not shown). The initial rates were calculated from the linear build-up of Fe(II) after the lag time. As shown in Fig. 2b, the initial, cell-normalized Fe(III) reduction rates were found to be proportional to the initial amounts of attached nanohematite. Linear regression of the data in Fig. 2b yielded a first-order rate constant of 3×10^{-3} h^{-1} for the reduction of nanohematite by *S. putrefaciens*.

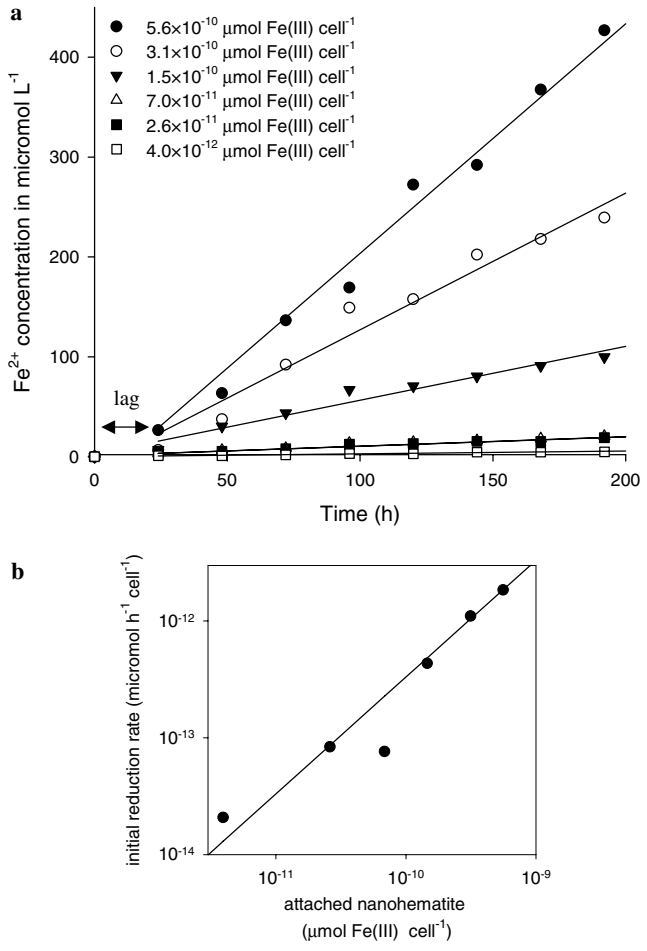

Fig. 2. (a) Build-up of Fe^{2+} concentration in cell–mineral incubations for variable amounts of nanohematite attached to *S. putrefaciens* cells. (b) Linear dependency of the initial iron reduction rate on the initial mass of cell-bound nanohematite. See text for complete description and discussion of the experiments.

4. Kinetic model of microbial reduction of Fe(III) colloids

The conceptual model for the reduction of Fe(III) colloids by *S. putrefaciens* is illustrated in Fig. 3. Reduction is assumed to occur via transfer of electrons from membrane-bound reductases to nearby Fe(III) centers at the surface of attached Fe(III) colloids. Far-field Fe(III) reduction, involving soluble electron shuttles, is not considered in the model. Therefore, the total reduction rate should reflect the abundance of Fe(III) colloids directly bound to the bacterial cells.

Based on the results presented in Fig. 1 for nanohematite, the model assumes that the partitioning of Fe(III) colloids to initially mineral-free cells of *S. putrefaciens* can formally be represented by a Langmuir isotherm:

$$\theta_B = \frac{[Fe^{III}_{cell}]}{BM_{max}} = \frac{K_P[Fe^{III}_{free}]}{1 + K_P[Fe^{III}_{free}]} \quad (1)$$

where θ_B represents the relative coverage of the cells by the colloids $[Fe^{III}_{free}]$ is the concentration of "free" colloidal particles, that is, particles not attached to cells, $[Fe^{III}_{cell}]$ is the concentration of colloids attached directly to the cells, M_{max} is the maximum attachment capacity per cell, B is the bacterial density per unit volume suspension, and K_P is the attachment constant.

Assuming a homogenous distribution of reductase sites at the cell surface, plus a uniform size of the iron colloids, the number of reaction centers for electron transfer should be proportional to the relative coverage of the cells, θ_B. The initial Fe(III) reduction rate is then given by:

$$R = -\frac{d[Fe^{III}_{tot}]}{dt} = kBM_{max}\theta_B = \frac{kBM_{max}[Fe^{III}_{free}]}{\frac{1}{K_P} + [Fe^{III}_{free}]} \quad (2)$$

where k is a first-order reduction rate constant and $[Fe^{III}_{tot}]$ is the total (initial) concentration of Fe(III) colloids in units of mass Fe(III) per unit volume total suspension. According to Eq. (2), the maximum cell-normalized iron reduction rate, v_{max}, is:

$$v_{max} = kM_{max} \quad (3)$$

Combining Eqs. (2) and (3), and defining the reciprocal value of K_P as K_m, results in:

$$R = \frac{v_{max}B[Fe^{III}_{free}]}{K_m + [Fe^{III}_{free}]} \quad (4)$$

Eq. (4) is formally identical to the Michaelis–Menten rate equation with $[Fe^{III}_{free}]$ as the substrate concentration. Direct application of Eq. (4) to data sets on microbial Fe(III) reduction, however, is hindered by the fact that usually the total, rather than the "free", concentration of the Fe(III) substrate is known (for examples, see, Roden and Zachara, 1996; Bonneville et al., 2004). Furthermore, in many circumstances it may not be appropriate to approximate the concentration of free Fe(III) colloids by the total Fe(III) concentration. For instance, in the case of nanohematite, at low mineral-to-cell ratios, the majority of particles are attached to the cells (Section 3.1). Under these circumstances, $[Fe^{III}_{free}]$ represents only a fraction of $[Fe^{III}_{tot}]$.

In systems where the partitioning of Fe(III) colloids can be described by Eq. (1), incorporation of the mass balance for ferric iron $[Fe^{III}_{tot}] = [Fe^{III}_{free}] + [Fe^{III}_{cell}]$ into Eq. (1) yields a

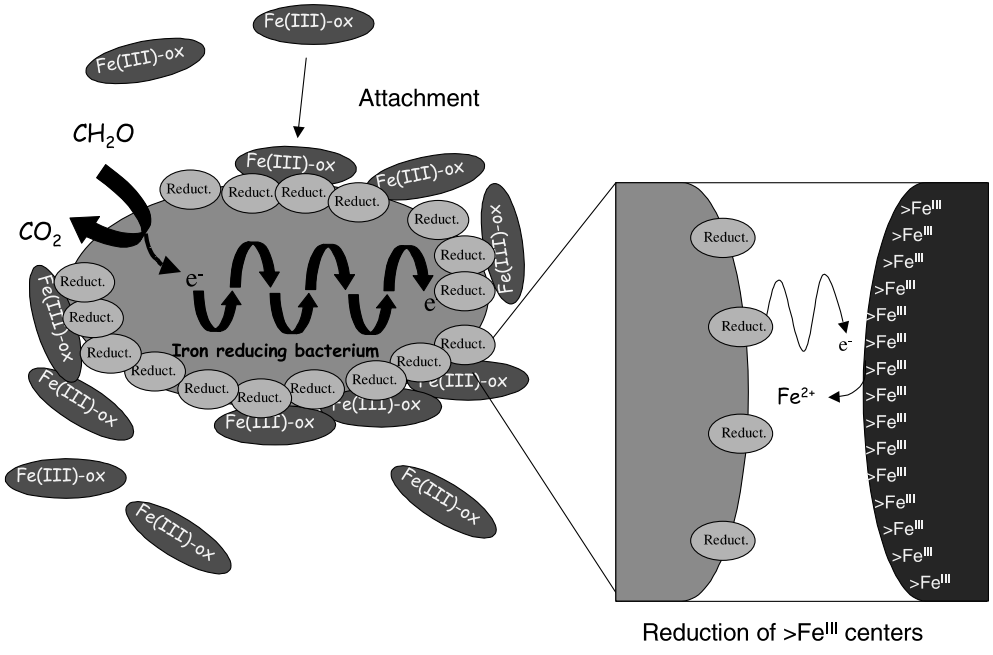

Fig. 3. Conceptual model of the reduction of Fe(III) colloids by *S. putrefaciens*. The reduction process consists of two consecutive steps: (1) attachment of the Fe(III) colloids to the iron reducing microorganism and (2) reduction of Fe(III) centers at the surface of attached colloids by electron transfer from membrane-bound Fe(III) reductases (indicated as "Reduct.").

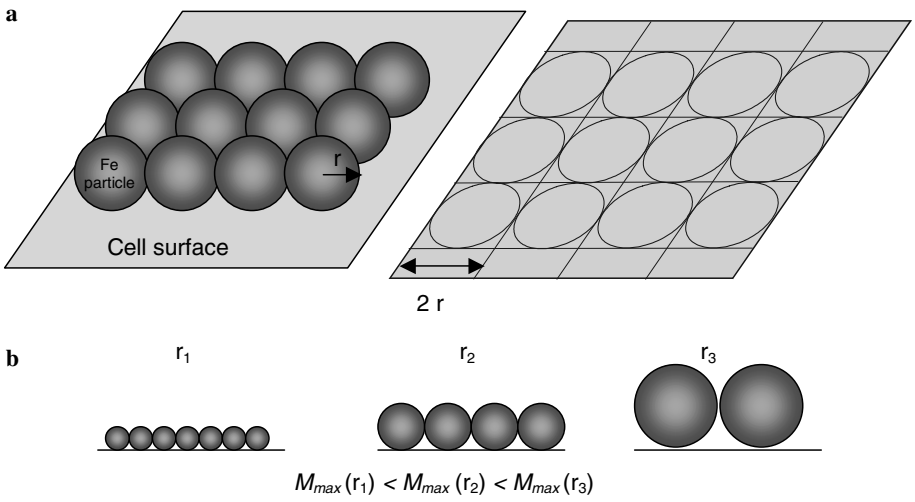

Fig. 4. (a) Geometric estimation of the maximum mass of Fe(III) colloids, M_{max}, that can bind directly to the cell surface, assuming a cubic packing of the colloids. (b) Particle size dependency of M_{max}.

quadratic equation in $[Fe^{III}_{free}]$. Combining the solution to the quadratic equation with Eq. (4), we then obtain:

$$R = k\frac{1 + A + C - \sqrt{1 + A(2 + A - 2C) + C(2 + C)}}{2K_P} \quad (5)$$

where $A = K_P[Fe^{III}_{tot}]$ and $C = M_{max}\,BK_P$. In rate Eq. (5), the initial reduction rate is expressed as a function of the total initial concentration of Fe(III) colloids, $[Fe^{III}_{tot}]$, and the cell density, B. The equation contains three adjustable parameters, k, K_P, and M_{max}, which are specific for the Fe(III) colloid–microbe system under consideration.

Assuming that only the Fe(III) centers in direct contact with the cell membrane are susceptible of being reduced, the maximum capacity, M_{max}, in rate Eq. (5) should reflect the size of the Fe(III) colloids, relative to that of the cells (Fig. 4). For colloids that are much smaller than the cells (as in the case of nanohematite), a simple geometrical estimate of M_{max} can be calculated as:

$$M_{max} = \frac{n_{Fe}V_P\rho}{M_P} \times \frac{A_B}{A_P} \quad (6)$$

where A_B is the surface area of the cell, while A_P is the projected surface area of a mineral particle onto the cell (Fig. 4a); V_p, ρ, M_P, are the volume, density, and molar mass of the Fe(III) colloids, and n_{Fe} is the number of iron atoms in the stoichiometric formula of the Fe(III) oxyhydroxide mineral. Fig. 4a illustrates how an order-of-magnitude estimate of M_{max} can be derived for spherical colloids, assuming a simple, two-dimensional cubic surface packing of the colloids.

It is important to note that the above rate model applies to the initial stage of reduction, when the amount of Fe(III) reduced is negligible compared to the total amount of Fe(III) initially present. Upon desorption of a reduced Fe(II) ion from the surface of a cell-bound Fe(III) colloid, an underlying Fe(III) center is exposed, which, in turn, becomes available for reduction. This recycling mechanism ensures that the concentration of Fe(III) centers at the bacterium–mineral interface remains initially constant, justifying the steady-state assumption for $[Fe^{III}_{cell}]$ implied in the derivation of the rate law. To describe iron reduction kinetics beyond the initial stage of reduction, one would need to account for the decrease of Fe(III) particles size during dissolution (Larsen and Postma, 2001), as well as for the progressive loss of cell viability and the accumulation of Fe(II) in the system (Roden and Urrutia, 2002).

5. Discussion

5.1. Nanohematite attachment to S. putrefaciens

The kinetic model presented in Section 4, couples the iron reduction rate to the relative coverage of the iron reducing bacteria by Fe(III) colloids. In particular, the assumption that attachment of the colloids to the cells follows a Langmuir isotherm (Eq. (1)) implies that the half-saturation constant, K_m, appearing in rate Eq. (4) equals the reciprocal of the attachment constant, K_P, of the isotherm. Furthermore, the iron reduction rate approaches its maximum value when the cells approach monolayer coverage by Fe(III) colloids.

The Langmuir isotherm provides an adequate macroscopic description of the attachment of nanohematite to *S. putrefaciens* at pH 5 (Fig. 1). A progressive increase in cell coverage by nanohematite with increasing mineral loading is also apparent in electron micrographs of cells exposed to variable nanohematite concentrations (Fig. 5). As can be seen in Fig. 5, for very high nanohematite to cell ratios, the cells become surrounded by a near-continuous layer of attached Fe(III) colloids.

The maximum attachment capacity, M_{max}, measured in the attachment experiments at pH 5 (Fig. 1; $M_{max} = 1.1 \times 10^{-9}$ μmol Fe(III) cell^{-1}) is, as described in

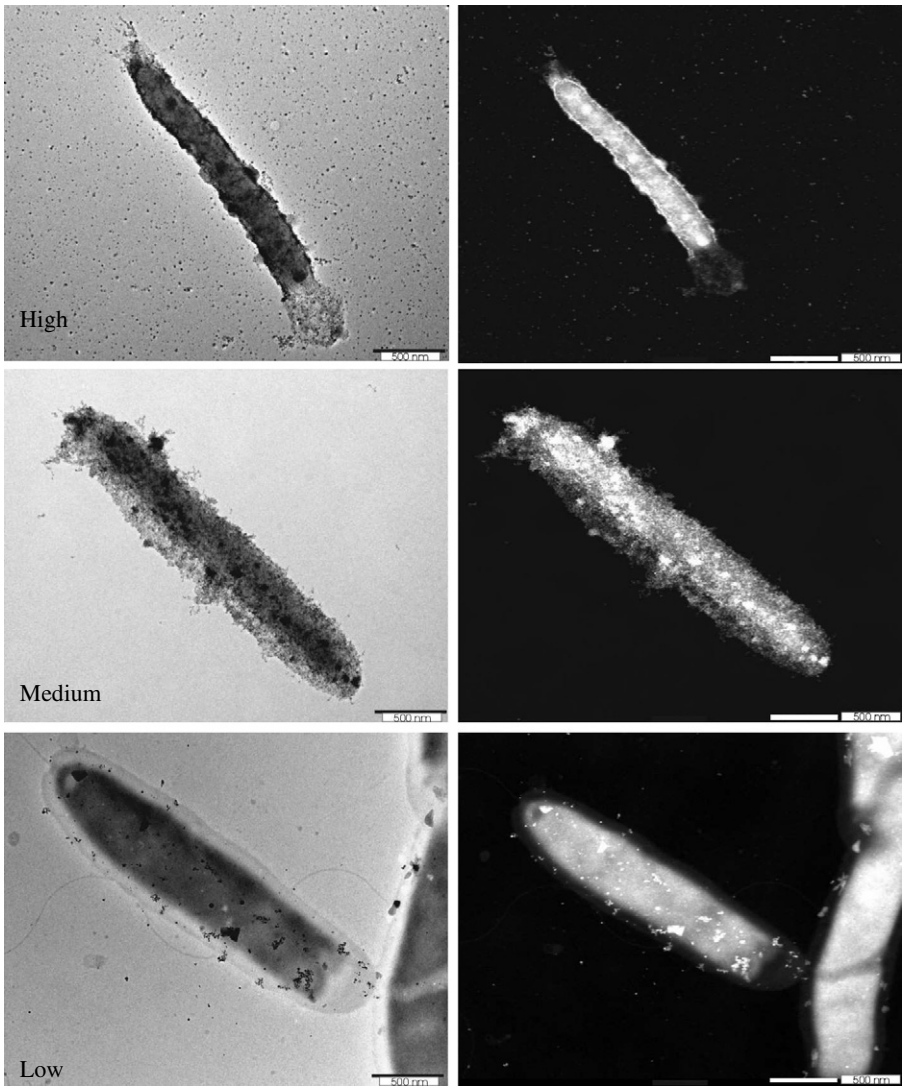

Fig. 5. TEM (right) and STEM (left) micrographs of *S. putrefaciens* cells that have been exposed to 20 (Low), 100 (Medium), and 500 (High) μmol L^{-1} of nanohematite (cell density = 2×10^8 cells mL^{-1}, pH 7). The shrunken appearance of the bacteria at high and medium iron loads are due to longer exposure to the high vacuum environment inside the TEM compared to bacteria exposed to low nanohematite concentration.

the following, in good agreement with the value inferred from the relative sizes of the cells and Fe(III) colloids. A geometric surface area for *S. putrefaciens* of 8.3 ± 2.1 μm^2 is derived from the average ($n = 63$) diameter (0.7 ± 0.1 μm) and length (3.1 ± 0.7 μm) of intact bacterial cells observed with transmission electron microscopy. With this surface area, and assuming an average diameter of 8 nm for the nanohematite particles (Section 2.1), a density of hematite of 5.26 g cm^{-3}, and a cubic packing of the Fe(III) colloids on the cell wall (Fig. 4a), Eq. (6) yields $M_{max} = 2.3 \times 10^{-9}$ μmol Fe(III) $cell^{-1}$. This value falls within a factor of two of that obtained independently from the attachment experiments, that is, well within the uncertainties of both estimations of M_{max}.

Strictly speaking, the Langmuir isotherm applies to reversible adsorption reactions of molecular species to two-dimensional surfaces, that is, processes that differ fundamentally from the adhesion of mineral particles to bacterial cell walls. Thus, the Langmuir isotherm is used here as an empirical equation that accounts for the observed saturation behavior of the concentration of cell-bound nanohematite. Similarly, Das and Caccavo (2001) found that the attachment of bacterial cells to large iron oxide particles could be described by a Langmuir isotherm.

Electrophoretic mobility measurements and acid–base titrations show that *S. putrefaciens* cells carry a net negative charge at pH $\geqslant 4$ (Claessens et al., 2004). In contrast, nanohematite is positively charged at pH 5, given its pH of zero net proton charge of 8.15 (Liger et al., 1999). Consequently, under the conditions of the attachment experiments (pH 5 and low ionic strength), electrostatic repulsion among nanohematite particles and coulombic attraction between nanohematite particles and bacteria facilitates the attachment of the Fe(III) colloids to the cells. The available evidence, however, indicates that short-range, non-coulombic interactions, that is, hydrogen bonds

and dipole–dipole interactions, play a major role in irreversibly binding the nanohematite particles to the cells.

Cells of *Shewanella* species can apparently synthesize specific proteins that enhance adhesion of Fe(III) oxyhydroxide particles (Caccavo, 1999; Lower et al., 2000; Lower et al., 2001). Even in the absence of specifically synthesized proteins, however, non-coulombic interactions between structural components of the outer cell wall of Gram-negative bacteria and Fe(III) oxide minerals likely generate strong attractive forces at short distances. In particular, the flexible O side chain of lipopolysaccharides, a major constituent of the outer membrane of Gram-negative bacteria, may account for the "non-specific" attractive forces measured upon retraction of *Shewanella oneidensis* from Fe(III) oxyhydroxide mineral surfaces (Lower et al., 2001). The absence of significant release of attached nanohematite in pH range 5–9 (Section 3.1) further implies that strong, non-coulombic forces maintain the colloidal particles attached to the cells.

5.2. Microbial reduction of nanohematite

Several outer-membrane *c*-type cytochromes capable of mediating electron transfer to Fe(III) and Mn(IV) oxides have been isolated from *Shewanella* cultures (Arnold et al., 1988; Myers and Myers, 1997; Beliaev and Saffarini, 1998; Caccavo, 1999; Blakeney et al., 2000). Their abundance depends on the growth conditions of the bacteria, with values of 0.45×10^{-2} and 1.96×10^{-2} μmol *c*-type cytochrome per mg of protein reported for cultures of *S. putrefaciens* 200 grown under aerobic and microaerobic conditions, respectively (Picardal et al., 1993). Based on the average protein content of *S. putrefaciens* 200R cells grown aerobically in LB medium (56% of the cell dry weight, Bin Lin, Free University of Amsterdam, personal communication), and their dry cell mass (3×10^{-13} g cell^{-1}), a *S. putrefaciens* cell should contain on the order of 7×10^{-19} mol of *c*-type cytochromes. If these cytochromes can be assimilated to reduction sites for Fe(III) then, for an estimated cell surface area of 8.3 μm^2 (Section 5.1), we obtain a density of 0.054 sites per nm^2, or an average of about three reductase sites per cell-bound nanohematite particle. The reductase abundance is thus sufficient to insure that every nanohematite particle becomes a potential electron acceptor upon attachment to the cell surface.

As the coverage of the outer membrane by nanohematite increases, so does the number of reaction centers for electron transfer from the cell to Fe(III) (Fig. 3). Irrespective of the details of the reaction mechanism, the overall Fe(III) reduction rate should then also increase. This model prediction is verified by the observed proportionality between the initial Fe(III) reduction rate and the surface coverage of the cells by nanohematite (Fig. 2b).

In order to determine the dependence of the iron reduction rate on the amount of attached Fe(III) colloids, the cells were first exposed to pH 5 nanohematite suspensions prior to initiating reduction at pH 7 (Section 2.3). In general, however, iron reduction experiments are started by directly introducing the cells in suspensions of Fe(III) oxyhydroxides at circumneutral pH. The reduction kinetics, however, differ whether the cells are initially exposed to acidic conditions or not, as shown by comparing the first-order reduction rate constant obtained here ($k=3\times10^{-3}$ h^{-1}, Section 3.2) with that derived from the study of Bonneville et al. (2004). In the latter study, reduction of nanohematite by *S. putrefaciens* yielded $v_{max}=2.4\times10^{-11}$ μmol h^{-1} cell^{-1}. Combining this value of v_{max} with that of M_{max} (2.3×10^{-9} μmol cell^{-1}) in Eq. (3), results in a higher rate constant, $k=1.0\times10^{-2}$ h^{-1}. The slower iron reduction kinetics observed here likely reflects a loss of viability of *S. putrefaciens* cells when exposed to acidic conditions, as reported by Claessens et al. (2004, 2006).

In microbial iron reduction experiments where cells and Fe(III) oxyhydroxide colloids are directly brought together at near-neutral pH, aggregation of the mineral particles may take place. Because in the proposed model only Fe(III) centers located at the mineral–cell interface are potential electron acceptors (Fig. 3), aggregation should have little effect on M_{max}. That is, for a given cell size, the maximum number of Fe(III) particles that can attach directly to the cells still depends principally on the shape and size of the individual mineral particles. In contrast, deviations in the attachment constant, K_P, may be expected because, at near-neutral pH, attachment of Fe colloids to the cells now competes with attachment to other Fe(III) colloids.

5.3. Half-saturation constants

Bonneville et al. (2004) fitted initial reduction rates of a variety of fine-grained Fe(III) oxyhydroxide minerals by *S. putrefaciens* to a rate expression of the form of Eq. (4), but using the total Fe(III) concentration, $[Fe^{III}_{tot}]$, as the substrate concentration:

$$R=\frac{v_{max}B[Fe^{III}_{tot}]}{K^{*}_{m}+[Fe^{III}_{tot}]} \tag{7}$$

Given the high affinities of the Fe(III) oxides for the cells, $[Fe^{III}_{tot}]$ is expected to deviate significantly from the concentration of non-attached particles, $[Fe^{III}_{free}]$, especially at low mineral to cell ratios. The fitted half-saturation constants, K^{*}_{m}, should therefore be regarded as conditional parameters. Indeed, the optimized values of K^{*}_{m} reported by Bonneville et al. (2004) depend on the mineral to cell ratio. As shown below, such a dependence is predicted by the kinetic model presented in Section 4.

Model-derived rates of iron reduction are plotted in Fig. 6a as a function of the total Fe(III) concentration, for variable cell densities (10^6 up to 10^{10} cells mL^{-1}). The reduction rates are calculated using Eq. (5), which relates v ($=R/B$),the cell-normalized reduction rate, to $[Fe^{III}_{tot}]$. A constant value of K_P of 10^{-3} L μmol^{-1} is imposed, and the Fe(III) particles are assumed to be spherical with a

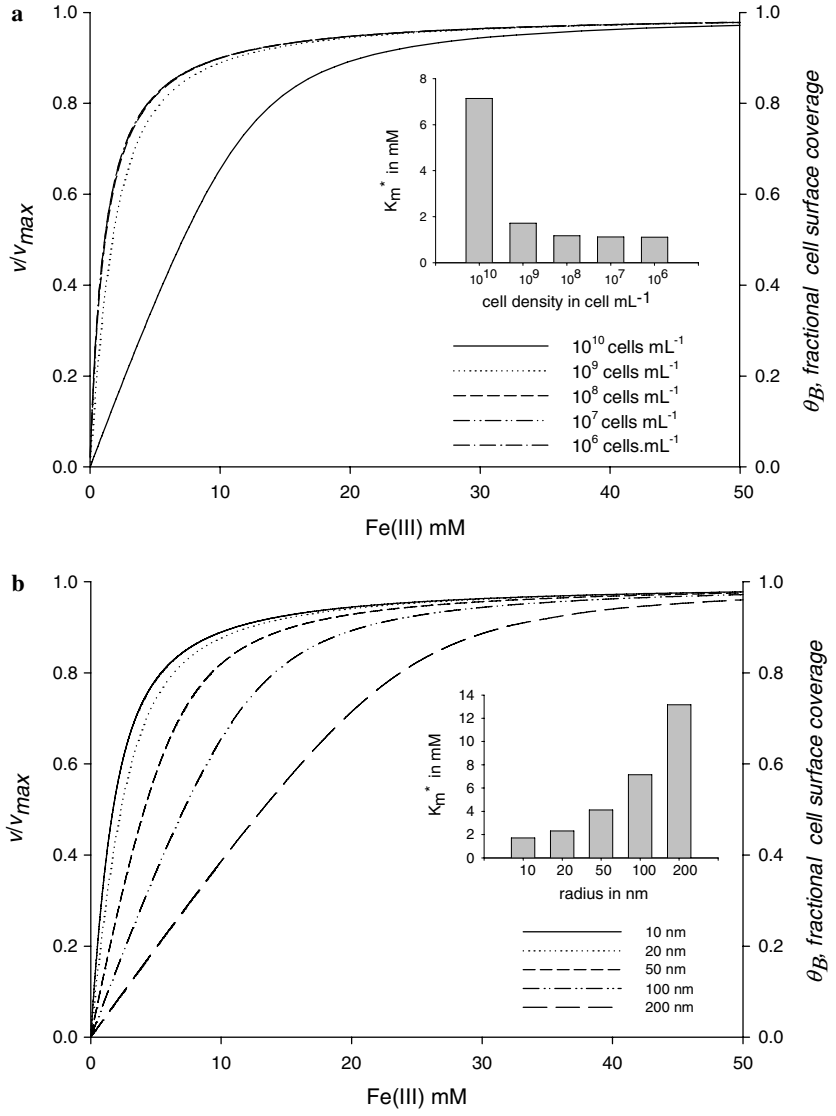

Fig. 6. Model-predicted microbial iron reduction kinetics for spherical Fe(III) colloids, as a function of cell density (a) and particle diameter (b). See text for details.

diameter of 10 nm. For all cell densities considered, the model-derived iron reduction rates exhibit a Michaelis–Menten-type dependence on the total Fe(III) concentration (Fig. 6a). At low to intermediate cell densities (10^6–10^8 cells mL^{-1}), the v versus $[Fe^{III}_{tot}]$ curves are nearly identical, and the apparent K^*_m values approach the intrinsic half-saturation constant, $K_m = 1/K_P$. At the higher cell densities (10^9 and 10^{10} cells mL^{-1}), K^*_m values exceed K_m. This is because, at a given $[Fe^{III}_{tot}]$, the relative coverage of individual cells by Fe(III) colloids, θ_B, decreases with increasing cell density. It is important to stress that the higher K^*_m values at the higher cell to mineral ratios are not due to a decrease in the affinity of the Fe(III) particles for attachment to the cells, but to a change in the partitioning of $[Fe^{III}_{tot}]$ between cell-bound and free Fe(III) particles.

For practical reasons, the Fe(III) substrate availability is expressed in mass-based concentration units. However, the actual Fe(III) centers that undergo reduction are located at the surface of Fe(III) particles attached to the cells. Because particle mass and surface area are not linearly related, apparent half-saturation constants should also depend on particle size. This is shown in Fig. 6b, where iron reduction rates calculated for a fixed bacterial density (5×10^8 cells mL^{-1}) and a fixed value of K_P (10^{-3} L μmol^{-1}) are plotted. The spherical Fe(III) colloids are assigned diameters varying from 10 to 200 nm. With increasing particle size, the model predicts increasing K^*_m values, because of decreasing mineral–cell contact area. Again, the observed variability in K^*_m reflects apparent, rather than true, changes in the attachment affinity of the mineral particles for the cells.

5.4. Application to other Fe(III) oxyhydroxide

The kinetic model successfully reproduces the observed saturation of the rate of nanohematite reduction by *S. putrefaciens* with increasing mineral loading. A similar

behavior has been observed for the reductive dissolution of a number of other colloidal Fe(III) oxyhydroxides by *S. putrefaciens* (Bonneville et al., 2004). Thus, it seems reasonable to hypothesize that rate Eq. (5) provides a general description of the dependence of the reduction rate of Fe(III) colloids on the Fe(III) substrate concentration, $[Fe^{III}_{tot}]$, and the cell density, B.

As for nanohematite, the maximum mass of iron particles that can directly attach to the cell surface, M_{max}, is calculated based on the size, shape, and density of the Fe(III) oxyhydroxides (Table 1). The estimates of M_{max} vary by more than two orders of magnitude (Table 2). These variations reflect the large differences in size, and hence specific surface area, of the different minerals considered. By combining in Eq. (3) the estimates of M_{max} with the maximum cell-normalized reduction rates, v_{max}, reported by Bonneville et al. (2004), values for the first-order reduction rate constants, k, are obtained (Table 2). The rate constants range over four orders of magnitude with the highest value for amorphous hydrous ferric oxide (HFO) and the lowest for low surface area (LSA) hematite.

Table 2
Kinetic model parameters

Iron oxyhydroxide	M_{max} (μmol cell^{-1})	K_P (L μmol^{-1})	k (h^{-1})
Nanohematite	2.3×10^{-9}	1.1×10^{-3}	1.0×10^{-2}
6-Line ferrihydrite	8.6×10^{-10}	8.0×10^{-4}	9.4×10^{-2}
LSA hematite	2.6×10^{-8}	2.0×10^{-3}	1.0×10^{-4}
Lepidocrocite	1.5×10^{-8}	5.0×10^{-5}	1.3×10^{-3}
HFO	4.3×10^{-10}	1.0×10^{-3}	1.5×10^{-1}

Using the predetermined values of M_{max} and k, the only remaining adjustable parameter in rate Eq. (5) is the attachment constant K_P. For each Fe(III) oxyhydroxide phase, an optimized value of K_P is obtained by fitting Eq. (5) to the rates measured by Bonneville et al. (2004). As summarized in Fig. 7b, the kinetic model successfully reproduces the order-of-magnitude variations in iron reduction rates of the five oxyhydroxides, for variable Fe(III) substrate concentrations and bacterial cell densities.

The value of K_P derived for nanohematite from fitting Eq. (5) to the Fe(III) reduction rate data (1.1×10^{-3} L μmol^{-1}, Table 2) deviates from that determined in the attachment experiments (2.0×10^{-2} L μmol^{-1}, Section 3.1). This discrepancy is ascribed to differences in pH and ionic strength conditions. At the higher ionic strength (0.02 versus 0.005 M NaCl) and pH (7 versus 5) of the incubations of Bonneville et al. (2004), colloidal suspensions of nanoparticulate hematite are not stable and coagulation is observed. Therefore, the attachment of hematite nanoparticles to the cells competes with the attachment of the nanoparticles to one another. This competition should result in a lower value of attachment constant to the cells, K_P.

Similar values of K_P are obtained for all the oxyhydroxides, with the exception of lepidocrocite (Table 2). The order-of-magnitude smaller K_P value for lepidocrocite suggests a lower tendency of this mineral to attach to the

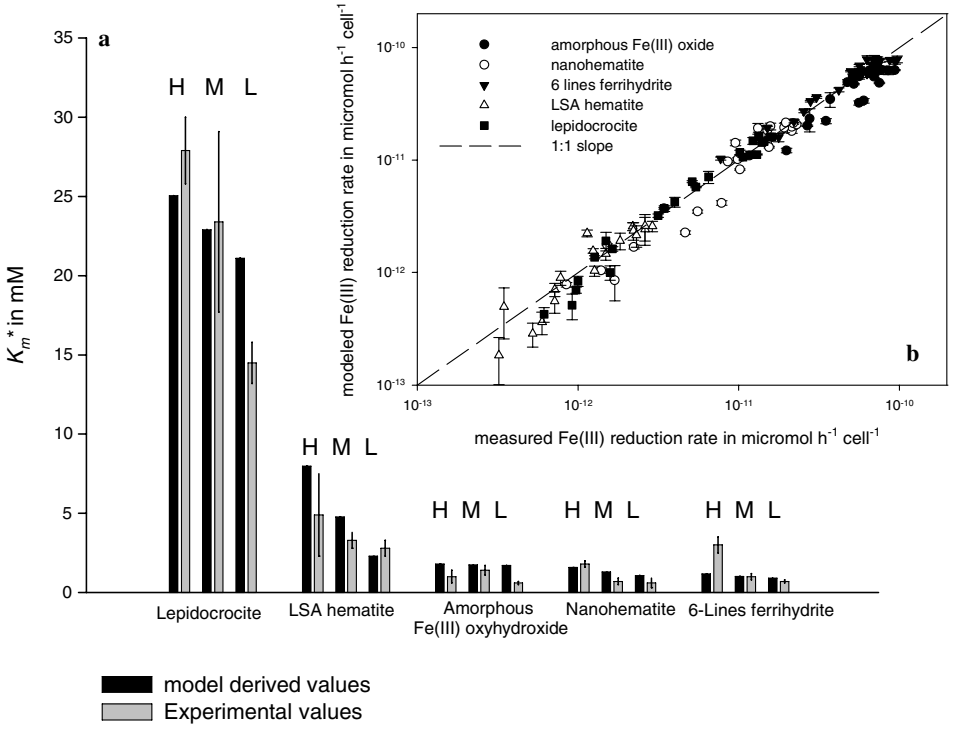

Fig. 7. Application of the proposed kinetic model to the reduction of different fine-grained Fe(III) oxyhydroxides by *S. putrefaciens*. (a) Apparent half-saturation constants, K_m^*, at three different bacterial densities, high (H), medium (M), and low (L), ranging from 1.1 to 7.6×10^8 cells mL^{-1}. (b) Modeled versus measured microbial iron reduction rates for the different Fe(III) oxyhydroxides considered (see Table 1). All data used were taken from Bonneville et al. (2004). See text for detailed discussion.

cells. Possibly, this is due to the elongated shape of the lepidocrocite (Table 1), which may interfere with a close packing of the particles at the bacterial surface. In contrast, all other Fe(III) colloids are spherical. Further studies are needed, however, to determine whether steric effects related to particle shape explain the deviating K_P value for lepidocrocite. It is important to note that the estimation of M_{max} via Eq. (6) is only valid when the oxyhydroxide particles are much smaller than the cells. For mineral particles exceeding the size of the cells, it is more appropriate to consider the isotherm describing the attachment of the bacteria to the mineral surface. The reduction rate would then be expressed in terms of the relative coverage of the available mineral surface by the cells.

From the optimized K_P values, it is possible to derive apparent K_m^* values as a function of the cell density (Section 5.3, Fig. 6a). The model-derived K_m^* values can then be compared directly to the values obtained experimentally for different bacterial cell densities in the study of Bonneville et al. (2004). As shown in Fig. 7a, the model correctly predicts the magnitudes of the K_m^* values, and reproduces the observed dependency of K_m^* on cell density.

5.5. Bioreduction kinetics and cell density

So far, emphasis has been on explaining the saturation of the rate of microbial iron reduction with respect to the concentration of the Fe(III) solid phase (e.g., Fig. 6). As shown by Roden and Zachara (1996) and Roden (2003), iron reduction rates also asymptotically approach maximum values when increasing the cell density in bacteria–mineral suspensions. This behavior is not directly apparent from Eqs. (2) and (4), which may seem to imply a linear dependence of the reduction rate on the cell density, B. This linear dependence, however, is only apparent, because, at a given total concentration of the Fe(III) colloids, the relative coverage of the cells, θ_B, is itself dependent on B.

To demonstrate that the kinetic model presented here reproduces the saturation of microbial Fe(III) reduction kinetics with increasing cell density, Eq. (5) is applied to the data for hydrous ferric oxide (HFO) reduction by *Shewanella alga* strain BrY reported in Roden and Zachara (1996). These authors measured initial iron reduction rates at constant bacterial density while varying the HFO concentration (Fig. 1 in Roden and Zachara, 1996), but also at constant HFO concentration while varying the cell density (Fig. 3 in Roden and Zachara, 1996). Eq. (5) is therefore first fitted to the reduction rates measured for variable HFO concentrations, assuming a mineral particle size of 6 nm. From the fit, a value for K_P of 2×10^{-5} L μmol^{-1} is obtained. Next, rate Eq. (5) is used to forecast HFO reduction rates as a function of cell density at a constant HFO concentration. The model-predicted rates are then compared to the measured rates.

The results of the initial model fit and the subsequent model forecast are shown in Fig. 8. The observed parabolic

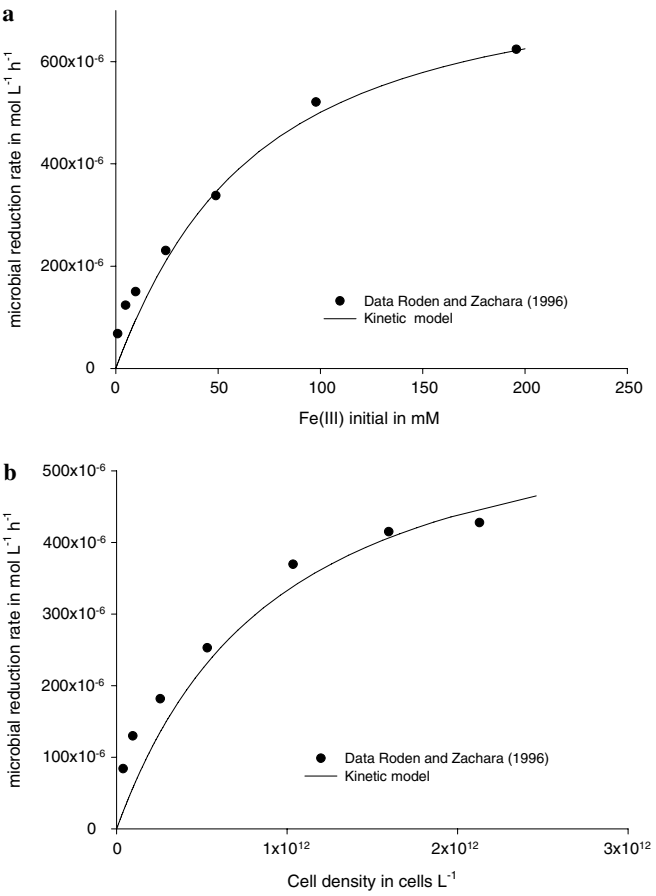

Fig. 8. Rates of hydrous ferric oxide (HFO) reduction by *S. alga* strain BrY. (a) Fit of Eq. (5) to rates measured at variable HFO concentrations and a fixed cell density of 2×10^8 cells mL^{-1}. (b) Model-predicted rates as a function of cell density, at a fixed HFO concentration of 20 mM Fe(III). All data are from Roden and Zachara (1996). See text for complete discussion.

dependence of the Fe(III) reduction rate on the HFO concentration (Fig. 8a) is similar to that found for the microbial reduction of HFO and other Fe(III) oxyhydroxides by Bonneville et al. (2004). Therefore, not surprisingly, the data in Fig. 8a can be fitted by Eq. (5). However, with the same set of model parameters, Eq. (5) also correctly predicts the observed dependence of the HFO reduction rate on the density of iron reducing bacterial cells (Fig. 8b).

6. Conclusions

The proposed kinetic model links the rate of enzymatic reduction kinetics of colloidal Fe(III) oxyhydroxides to the relative coverage of iron reducing cells by mineral particles. The experimental and modeling results highlight the central role of cell–mineral adhesion processes in the reduction of solid phase Fe(III) by *S. putrefaciens*, and the need for a better understanding of their molecular nature. The model captures a number of essential features of iron reduction kinetics in mixed cell–mineral suspensions, in particular, the observed saturation of the bioreduction rate with re-

spect to both the solid phase Fe(III) substrate concentration (Bonneville et al., 2004) and the cell density (Roden and Zachara, 1996). The model further accounts for the particle size dependency of the microbial reduction of Fe(III) colloids.

The idealized experimental system considered clearly does not account for all the complexity of microbial iron reduction in natural environments. The proposed kinetic model, for instance, does not address the key role played by the bioavailability of potential electron donors (Lovley et al., 1989; Petruzzelli et al., 2005), the physical accessibility of Fe(III) minerals to iron reducers (Zachara et al., 1998), or the community structure and ecology of resident microbial populations (Röling et al., 2001). In addition, the model applies specifically to iron reduction requiring direct cell–mineral attachment, which, itself, depends on a variety of parameters, such as pH, ionic strength, cell physiology, and the structure of the bacterial membrane. Further work is thus needed to incorporate the results of this study into a broader kinetic framework describing microbial Fe(III) reduction activity in environmental systems.

Acknowledgments

This study is part of TRIAS project 835.80.004, co-funded by the Centre for Soil and Quality Management and Knowledge Transfer (SKB), Delft Cluster (DC), and the Council for the Earth and Life Sciences (ALW) of the Netherlands Organization for Scientific Research (NWO). The authors thank Hans Meeldijk (Group of Inorganic Chemistry and Catalysis, Department of Chemistry, Utrecht University) for the TEM and STEM micrographs. We are also grateful to the Associate Editor, Dr. J. Haas, and three anonymous referees for their constructive reviews.

Associate editor: Johnson R. Haas

References

Albrechtsen, H.-J., Christensen, T.H., 1994. Evidence for microbial iron reduction in a landfill leachate-polluted aquifer (Vejen, Denmark). *Appl. Environ. Microbiol.* **60**, 3920–3925.

Anderson, R.T., Lovley, D.R., 1999. Naphthalene and benzene degradation under Fe(III)-reducing conditions in petroleum-contaminated aquifers. *Biorem. J.* **3**, 121–135.

Arnold, R.G., DiChristina, T.J., Hoffmann, M.R., 1988. Reductive dissolution of iron(III) oxides by *Pseudomonas* sp. 200. *Biotechnol. Bioeng.* **32**, 1081–1096.

Behrends, T., Van Cappellen, P., 2005. Competition between enzymatic and abiotic reduction of uranium(VI) under iron reducing conditions. *Chem. Geol.* **220**, 315–327.

Beliaev, A.S., Saffarini, D.A., 1998. *Shewanella putrefaciens* mtrB encodes an outer membrane protein required for Fe(III) and Mn(IV) reduction. *J. Bacteriol.* **180**, 6292–6297.

Blakeney, M.D., Moulaei, T., DiChristina, T.J., 2000. Fe(III) reduction activity and cytochrome content of *Shewanella putrefaciens* grown on ten compounds as sole terminal electron acceptor. *Microbiol. Res.* **155**, 87–94.

Bonneville, S., Van Cappellen, P., Behrends, T., 2004. Microbial reduction of iron(III) oxyhydroxides: effects of mineral solubility and availability. *Chem. Geol.* **212**, 255–268.

Caccavo Jr., F., 1999. Protein-mediated adhesion of the dissimilatory Fe(III)-reducing bacterium *Shewanella alga* BrY to hydrous ferric oxide. *Appl. Environ. Microbiol.* **65**, 5017–5022.

Caccavo, F.J., Das, A., 2002. Adhesion of dissimilatory Fe(III)-reducing bacteria to Fe(III) minerals. *Geomicrobiol. J.* **19**, 161–177.

Canfield, D.E., Thamdrup, B., Hansen, J.W., 1993. The anaerobic degradation of organic matter in Danish coastal sediments: iron reduction, manganese reduction, and sulfate reduction. *Geochim. Cosmochim. Acta* **57**, 3867–3883.

Claessens, J., Behrends, T., Van Cappellen, P., 2004. What do acid–base titrations of live bacteria tell us? A preliminary assessment. *Aquat. Sci.* **66**, 19–26.

Claessens, J., van Lith, Y., Laverman, A.M., Van Cappellen, P., 2006. Acid–base activity of live bacteria: implications for quantifying cell wall charge. *Geochim. Cosmochim. Acta* **70**, 267–276.

Cummings, D.E., Caccavo Jr., F., Fendorf, S., Rosenzweig, R.F., 1999. Arsenic mobilization by the dissimilatory Fe(III)-reducing bacterium *Shewanella alga* BrY. *Environ. Sci. Technol.* **33**, 723–729.

Das, A., Caccavo Jr., F., 2000. Dissimilatory Fe(III) oxide reduction by *Shewanella alga* BrY requires adhesion. *Curr. Microbiol.* **40**, 344–347.

Das, A., Caccavo Jr., F., 2001. Adhesion of the dissimilatory Fe(III)-reducing bacterium *Shewanella alga* BrY to crystalline Fe(III) oxides. *Curr. Microbiol.* **42**, 151–154.

DiChristina, T.J., DeLong, E.F., 1994. Isolation of anaerobic respiratory mutants of *Shewanella putrefaciens* and genetic analysis of mutants deficient in anaerobic growth on Fe^{3+}. *J. Bacteriol.* **176**, 1468–1474.

DiChristina, T.J., Moore, C.M., Haller, C.A., 2002. Dissimilatory Fe(III) and Mn(IV) reduction by *Shewanella putrefaciens* requires ferE, a homolog of the pulE (gspE) type II protein secretion gene. *J. Bacteriol.* **184**, 142–151.

Hobbie, J.E., Daley, R.J., Jasper, S., 1977. Use of nuclepore filters for counting bacteria by fluorescence microscopy. *Appl. Environ. Microbiol.* **33**, 1225–1228.

Kappler, A., Benz, M., Schink, B., Brune, A., 2004. Electron shuttling via humic acids in microbial iron(III) reduction in a freshwater sediment. *FEMS Microbiol. Ecol.* **47**, 85–92.

Larsen, O., Postma, D., 2001. Kinetics of reductive bulk dissolution of lepidocrocite, ferrihydrite and goethite. *Geochim. Cosmochim. Acta* **65**, 1367–1379.

Liger, E. 1996. Rôle catalytique des oxyhydroxides de Fe(III): Réduction de U(VI) par le Fe(II) adsorbé, Université Joseph Fourier, Grenoble, France. p. 187.

Liger, E., Charlet, L., Van Cappellen, P., 1999. Surface catalysis of uranium (VI) reduction by iron(II). *Geochim. Cosmochim. Acta* **63**, 2939–2955.

Lovley, D.R., Coates, J.D., 1997. Bioremediation of metal contamination. *Curr. Opin. Biotech.* **8**, 285–289.

Lovley, D.R., Giovannoni, S.J., White, D.C., Champine, J.E., Phillips, E.J.P., Gorby, Y.A., Goodwin, S., 1993. *Geobacter metallireducens* gen. nov. sp. nov., a microorganism capable of coupling the complete oxidation of organic compounds to the reduction of iron and other metals. *Arch. Microbiol.* **159**, 336–344.

Lovley, D.R., Phillips, E.J.P., Lonergan, D.J., 1989. Hydrogen and formate oxidation coupled to dissimilatory reduction of iron or manganese by *Alteromonas putrefaciens*. *Appl. Environ. Microbiol.* **55**, 700–706.

Lower, S.K., Hochella Jr., M.F., Beveridge, T.J., 2001. Bacterial recognition of mineral surfaces: nanoscale interactions between *Shewanella* and FeOOH. *Science* **292**, 1360–1363.

Lower, S.K., Tadanier, C.J., Hochella Jr., M.F., 2000. Measuring interfacial and adhesion forces between bacteria and mineral surfaces with biological force microscopy. *Geochim. Cosmochim. Acta* **64**, 3133–3139.

McCormick, M.L., Bouwer, E.J., Adriaens, P., 2002. Carbon tetrachloride transformation in a model iron-reducing culture: relative

kinetics of biotic and abiotic reactions. *Environ. Sci. Technol.* **36**, 403–410.

Myers, C.R., Myers, J.M., 1997. Outer membrane cytochromes of *Shewanella putrefaciens* MR-1: spectral analysis, and purification of the 83-kDa *c*-type cytochrome. *Biochim. Biophys. Acta* **1326**, 307–318.

Petruzzelli, L., Celi, L., Ajmone-Marsan, F., 2005. Effects of soil organic fractions on iron oxide biodissolution under anaerobic conditions. *Soil Sci.* **170**, 102–109.

Picardal, F.W., Arnold, R.G., Couch, H., Little, A.M., Smith, M.E., 1993. Involvement of cytochromes in the anaerobic biotransformation of tetrachloromethane by *Shewanella putrefaciens* 200. *Appl. Environ. Microbiol.* **59**, 3763–3770.

Roden, E.E., 2003. Fe(III) oxide reactivity toward biological versus chemical reduction. *Environ. Sci. Technol.* **37**, 1319–1324.

Roden, E.E., Urrutia, M.M., 2002. Influence of biogenic Fe(II) on bacterial crystalline Fe(III) oxide reduction. *Geomicrobiol. J.* **19**, 209–251.

Roden, E.E., Zachara, J.M., 1996. Microbial reduction of crystalline iron(III) oxides: influence of oxide surface area and potential for cell growth. *Environ. Sci. Technol.* **30**, 1618–1628.

Röling, W.F.M., van Breukelen, B.M., Braster, M., Bin, L., van Verseveld, H.W., 2001. Relationships between microbial community structure and hydrochemistry in a landfill leachate-polluted aquifer. *Appl. Environ. Microbiol.* **67**, 4619–4629.

Taillefert, M., Bono, A.B., Luther III., G.W., 2000. Reactivity of freshly formed Fe(III) in synthetic solutions and (pore)waters: voltammetric evidence of an aging process. *Environ. Sci. Technol.* **34**, 2169–2177.

Viollier, E., Inglett, P.W., Hunter, K., Roychoudhury, A.N., Van Cappellen, P., 2000. The ferrozine method revisited: Fe(II)/Fe(III) determination in natural waters. *Appl. Geochem.* **15**, 785–790.

Zachara, J.M., Fredrickson, J.K., Li, S.-M., Kennedy, D.W., Smith, S.C., Gassman, P.L., 1998. Bacterial reduction of crystalline Fe^{3+} oxides in single phase suspensions and subsurface materials. *Am. Mineral.* **83**, 1426–1443.

Zachara, J.M., Fredrickson, J.K., Smith, S.C., Gassman, P.L., 2001. Solubilization of Fe(III) oxide-bound trace metals by a dissimilatory Fe(III) reducing bacterium. *Geochim. Cosmochim. Acta* **65**, 75–93.